Journal of Solid State Chemistry 182 (2009) 1694–1699

Contents lists available at ScienceDirect

Journal of Solid State Chemistry

journal homepage: www.elsevier.com/locate/jssc

Magnetic properties of orthorhombic fluorite-related oxides Ln_3SbO_7 (Ln = rare earths)

Yukio Hinatsu *, Haruka Ebisawa, Yoshihiro Doi

Division of Chemistry, Graduate School of Science, Hokkaido University, Sapporo 060-0810, Japan

ARTICLE INFO

Article history:
Received 7 December 2008
Received in revised form
10 April 2009
Accepted 16 April 2009
Available online 23 April 2009

Keywords:
Magnetic properties
Rare earths
Oxides
Magnetic susceptibility
Specific heat
Antiferromagnetic transition

ABSTRACT

Ternary rare earth antimonates Ln_3SbO_7 (Ln = rare earths) were prepared and their structures were determined by X-ray diffraction measurements. They crystallize in an orthorhombic superstructure of cubic fluorite (space group $Cmcm$ for Ln = La, Pr, Nd; $C222_1$ for Ln = Nd–Lu), in which Ln^{3+} ions occupy two different crystallographic sites (the 8-coordinated and 7-coordinated sites). Their magnetic properties were characterized by magnetic susceptibility and specific heat measurements from 1.8 to 400 K. The Ln_3SbO_7 (Ln = Nd, Gd–Ho) compounds show an antiferromagnetic transition at 2.2–3.2 K. Sm_3SbO_7 and Eu_3SbO_7 show van Vleck paramagnetism. Measurements of the specific heat down to 0.4 K for Gd_3SbO_7 and the analysis of the magnetic specific heat indicate that the antiferromagnetic ordering of the 8-coordinated Gd ions occur at 2.6 K, and the 7-coordinated Gd ions order at a furthermore low temperature.

1. Introduction

Compounds of the general composition Ln_3MO_7 (Ln = rare earths, M = Nb, Ru, Ta, Re, etc.) have been attracting interest. They have an ordered, defect-fluorite superstructure. The relationship to the fluorite structure is as follows. The fluorite unit cell for oxides has the composition $M_4^{4+}O_8$. If the four tetravalent metal ions are replaced by three trivalent ions (Ln) and one pentavalent ion (M), one oxide vacancy is formed per fluorite cell. Due to the significant differences in radii between the Ln^{3+} and M^{5+} ions, cation ordering occurs on the metal sites and the oxide-vacancy orders on the anion sites. Rossell first determined the crystal structure of La_3NbO_7 [1]. It was well described in the orthorhombic space group $Cmcm$: M^{5+} ion is coordinated with six oxygen ions, forming a MO_6 octahedron. These octahedra share corners forming one-dimensional chains which are oriented along the c-axis. Although the space group for the La_3NbO_7 now turned out to be $Pnma$ [2], the space group $Cmcm$ has been applied for many Ln_3MO_7 compounds [3–26]. For some compounds such as Ln_3TaO_7 (Ln = Y, Sm–Ho) [20–22,24] and Ln_3MoO_7 (Ln = La–Nd, Sm, Eu) [27–30], the space groups $C222_1$ and $P2_12_12_1$ have been applied, respectively.

Due to this unique crystal structures and possible related magnetic properties, many studies have been performed, especially for the magnetic properties of compounds containing Ru^{5+} ion at the M-site because of its largest possible spin ($S = 3/2$) [3–13].

Another topic for Ln_3MO_7 is that detailed magnetic and thermal investigations on the ruthenium-, iridium- and osmium-containing members of the Ln_3MO_7 family show low-temperature structural phase transitions [9–11,13,14,19,26,29,31].

As for M = Sb compounds, a series of Ln_3SbO_7 with Ln = Nd, Sm–Yb, and Y was reported to have the pyrochlore structure [32]. However, Faurie et al. pointed out that the random distribution of Y^{3+} and Sb^{5+} required for the pyrochlore structure was unlikely on grounds of the different size and charge of the ions [33]. Rossell determined the crystal structure of Y_2GdSbO_7 with the space group $C222_1$ [1]. Later, IJdo et al. determined the structure for Pr_3SbO_7 with the space group $Cmcm$ [23]. Fennell et al. investigated the structure and magnetic properties of Ho_3SbO_7 and Dy_3SbO_7 [34]. They adopted the space group $C222_1$ for the two compounds. However, no atomic coordinates were presented for any of the compounds. A possibility of magnetically frustrated system was noted for Ho_3SbO_7 and Dy_3SbO_7 through magnetic susceptibility measurements. However, no systematic study on the crystal structure and magnetic properties of Ln_3SbO_7 has been carried out.

In this study, we successfully prepared a series of Ln_3SbO_7 from Ln = La to Lu. Through X-ray diffraction measurements, their crystal structures were determined. In order to elucidate magnetic properties and to check the existence of the phase transition in the Ln_3SbO_7 series, their magnetic susceptibility measurements from 1.8 to 400 K and the specific heat measurements from 0.4 to 400 K were performed.

* Corresponding author. Fax: +81 11 706 2702.
E-mail address: hinatsu@sci.hokudai.ac.jp (Y. Hinatsu).

0022-4596/$ - see front matter © 2009 Elsevier Inc. All rights reserved.
doi:10.1016/j.jssc.2009.04.015

2. Experimental

2.1. Sample preparation

As starting materials, rare earth oxides Ln_2O_3 (Ln = La, Nd, Sm–Gd, Dy–Lu), Pr_6O_{11}, Tb_4O_7, and Sb_2O_3 were used. For La_2O_3 and Nd_2O_3, they absorb moisture in air and easily form rare earth hydroxides $Ln(OH)_3$. Therefore, they were dried at 1173 K for 24 h before use. For better reactivity, mixtures of the rare earth oxides and Sb_2O_3 were dissolved in the concentrated nitric acid, and were heated first at 150 °C for one night and then at 600 °C for 6 h. These mixtures were pressed into pellets and heated at 1200 °C for 12 h. In the first stage of sample preparations, very small amounts of impurities remained in the desired compounds; they were unreacted starting materials Ln_2O_3. In order to remove these impurities, the samples were washed with diluted hydrochloric acid. After this treatment, single-phase Ln_3SbO_7 compounds could be obtained.

2.2. X-ray diffraction analysis

Powder X-ray diffraction profiles were measured using a Rigaku Multi-Flex diffractometer with Cu$K\alpha$ radiation equipped with a curved graphite monochromator. The data were collected by step-scanning in the angle range of $10^\circ \leqslant 2\theta \leqslant 120^\circ$ at a 2θ step-size of 0.02°. The X-ray diffraction data were analyzed by the Rietveld technique, using the programs RIETAN2000 [35].

2.3. Magnetic susceptibility measurements

The temperature dependence of the magnetic susceptibility was measured in an applied field of 0.1 T over the temperature range of 1.8 K $\leqslant T \leqslant$ 400 K, using a SQUID magnetometer (Quantum Design, MPMS5S). The susceptibility measurements were performed under both zero-field-cooled (ZFC) and field-cooled (FC) conditions. The former was measured upon heating the sample to 400 K under the applied magnetic field of 0.1 T after zero-field cooling to 1.8 K. The latter was measured upon cooling the sample from 400 to 1.8 K at 0.1 T.

2.4. Specific heat measurements

Specific heat measurements were performed using a relaxation technique by a commercial heat capacity measuring system (Quantum Design, PPMS) in the temperature range of 0.4–400 K. The sintered sample in the form of a pellet was mounted on a thin alumina plate with Apiezon for better thermal contact.

3. Results and discussion

3.1. Preparation and crystal structure

Except for Ln = Nd, all the Ln_3SbO_7 compounds (Ln = La, Pr, Sm–Lu) were obtained as a single phase. Fig. 1 shows the powder X-ray diffraction profiles for La_3SbO_7 and Sm_3SbO_7. Any of these diffraction patterns are similar to that for the fluorite structure and all reflections appeared to be consistent with the C-centered condition, $h+k = 2n$.

As described in the Introduction section, many space groups have been applied for the structure of Ln_3MO_7 compounds. Following earlier work on Pr_3SbO_7 and Y_2GdSbO_7 [1,23] we tried to analyze the crystal structures of Ln_3SbO_7 prepared in this study. The structure for La_3SbO_7 was well refined with the space group *Cmcm*. Table 1 lists the lattice parameters and atomic coordinates

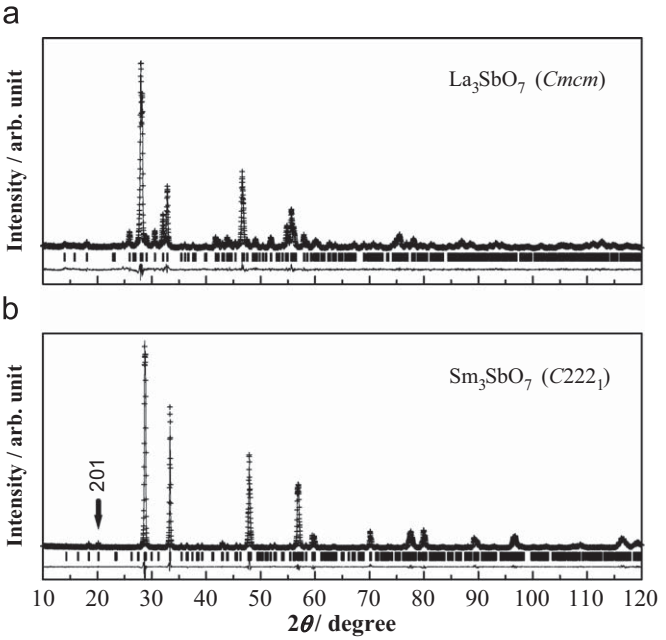

Fig. 1. Powder X-ray diffraction profiles for (a) La_3SbO_7 and (b) Sm_3SbO_7. The calculated and observed profiles are shown on the top solid line and cross markers, respectively. The vertical marks in the middle show positions calculated for Bragg reflections. The lower trace is a plot of the difference between calculated and observed intensities.

Table 1
Structural parameters for La_3SbO_7.

Atom	Site	x	y	z	B/Å^{2a}
La(1)	4*a*	0	0	0	0.52(4)
La(2)	8*g*	0.2275(1)	0.2972(2)	1/4	0.52
Sb	4*b*	0	1/2	0	0.30(4)
O(1)	16*h*	0.124(1)	0.326(1)	−0.036(1)	1.2(1)
O(2)	8*g*	0.134(2)	0.023(2)	1/4	1.2
O(3)	4*c*	0	0.431(2)	1/4	1.2

Note. Space group *Cmcm*; $a = 11.1300(9)$ Å, $b = 7.6398(6)$ Å, $c = 7.7399(6)$ Å, $V = 658.13(9)$ Å^3, $R_{wp} = 11.65\%$, $R_I = 2.82\%$ and $R_e = 8.62\%$, where $R_{wp} = [\sum_i w_i(y_i - f_i(x))^2/\sum_i w_i y_i^2]^{1/2}$, $R_I = \sum |I_k(o) - I_k(c)|/\sum I_k(o)$, and $R_e = [(N-P)/\sum_i w_i y_i^2]^{1/2}$.

for La_3SbO_7. The structure of La_3NbO_7 is reported to be better described with the space group *Pnma* than with *Cmcm* [2]. However, some extra reflection peaks which should be observed with the *Pnma* were not observed in the X-ray diffraction profile of La_3SbO_7. For the X-ray diffraction profiles of Ln_3SbO_7 (Ln = Sm–Lu), there exist many very weak $h\,0\,l$ reflections with odd l (see Fig. 1(b)), which could not be indexed based on the *Cmcm*. In addition to this, the C-centering extinction condition ruled out other space groups such as *Pnma* (for La_3NbO_7) [2] and $P2_12_12_1$ (for Ln_3MoO_7) [27–30]. This fact indicates that they have a different symmetry. We analyzed the X-ray diffraction profiles for Ln_3SbO_7 (Ln = Sm–Lu) with the space group $C222_1$. All the reflections observed could be successfully indexed. The refinement by using the structural model with the space group $C222_1$ converged rapidly, and yielded low residual factors and acceptably low values for the calculated standard deviations of refined parameters. Table 2 lists the lattice parameters and atomic coordinates for Sm_3SbO_7.

The X-ray diffraction profile for Nd_3SbO_7 indicated that the phase with the space group *Cmcm* and that with $C222_1$ coexist in

this compound at room temperature. We determined the ratio of the *Cmcm* phase and the $C222_1$ phase to be 44:56% by the Rietveld analysis.

Table 2
Structural parameters for Sm_3SbO_7.

Atom	Site	*x*	*y*	*z*	B/Å^{2a}
Sm(1)	4*b*	0	0.5063(9)	1/4	0.19(3)
Sm(2)	8*c*	0.2339(1)	0.2364(3)	−0.0015(5)	0.19
Sb	4*b*	0	−0.0008(9)	1/4	0.10(8)
O(1)	8*c*	0.138(3)	0.176(3)	0.250(2)	1.4(2)
O(2)	8*c*	0.112(2)	0.816(3)	0.324(3)	1.4
O(3)	4*a*	0.132(3)	1/2	0	1.4
O(4)	4*a*	0.131(3)	1/2	1/2	1.4
O(5)	4*a*	0.072(3)	0	0	1.4

Note. Space group $C222_1$; $a = 10.7280(4)$ Å, $b = 7.5506(3)$ Å, $c = 7.6048(3)$ Å, $V = 615.60(4)$ Å^3, $R_{wp} = 13.12\%$, $R_I = 3.94\%$, and $R_e = 9.81\%$.

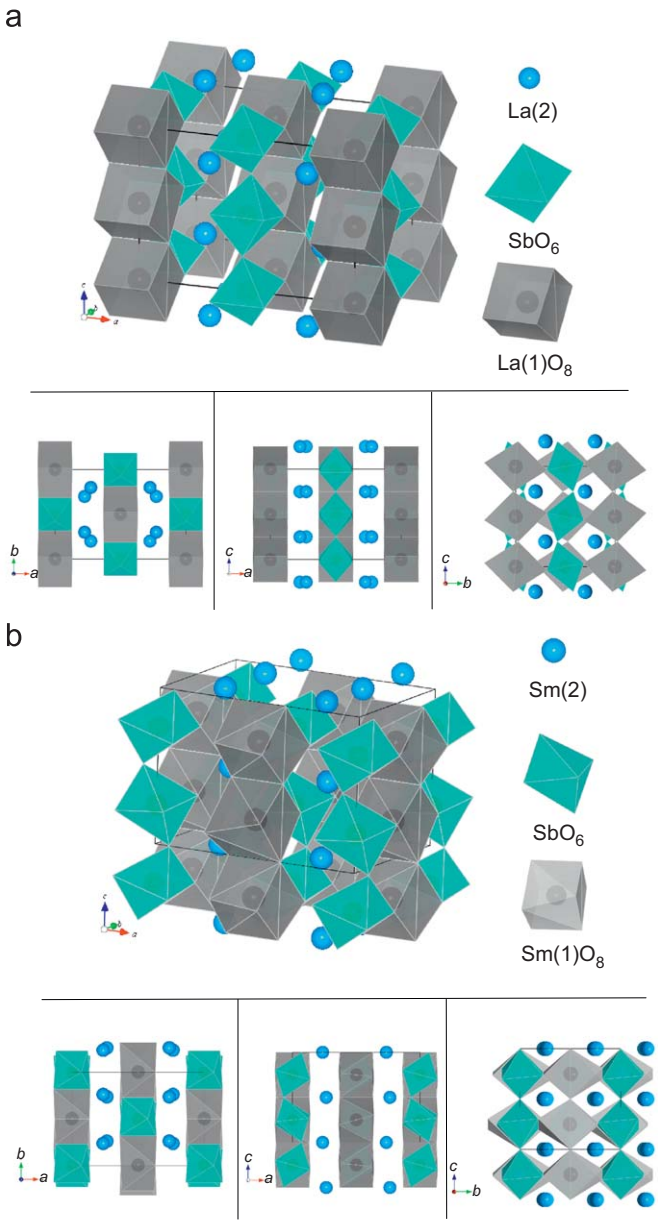

Fig. 2. Crystal structures of Ln_3SbO_7: (a) La_3SbO_7 (space group: *Cmcm*) and (b) Sm_3SbO_7 (space group: $C222_1$).

Fig. 2(a) and (b) illustrate the crystal structures determined for La_3SbO_7 and Sm_3SbO_7, respectively. The orthorhombic structures have features in common for both the compounds. The SbO_6 octahedra share the O(3) for La_3SbO_7 and O(5) for Sm_3SbO_7 ions, forming an infinite one-dimensional zig-zag chain parallel to the [001] direction. The *Ln*(1) ions are coordinated by eight oxygen ions and the distorted *Ln*(1)O_8 cubes also form a one-dimensional chain through edge-sharing. The SbO_6 and *Ln*(1)O_8 chains lie alternately parallel to the (100) plane, and the *Ln*(2) ions are 7-coordinated by oxygen ions between slabs consisting of these chains. The SbO_6 octahedron and *Ln*(1)O_8 cube in the La_3SbO_7 structure are more regular than those in the Sm_3SbO_7 structure. The SbO_6 octahedra in the La_3SbO_7 and Sm_3SbO_7 structures are tilted along the [100] and [010] directions, respectively.

Fig. 3 shows the variation of lattice parameters for Ln_3SbO_7 (*Ln* = La∼Lu) against the ionic radius of the 8-coordinated Ln^{3+} ion. The lattice parameters increase with the ionic radius of Ln^{3+} and the differences among the $a/\sqrt{2}$, *b*, and *c* values become wide. For the $C222_1$ phase, the *b* values are almost equal to the *c* values between *Ln* = Gd and Lu, and the *b* values become smaller than the *c* values from *Ln* = Eu to Nd. The differences among $a/\sqrt{2}$, *b*, and *c* for the *Cmcm* phase are larger than those for the $C222_1$ phase.

Fig. 4 shows the variation of the average *Ln*–O and Sb–O bond lengths with the ionic radius of 8-coordinated Ln^{3+} ion. The average bond lengths *Ln*(1)–O and *Ln*(2)–O both increase with the ionic radius of Ln^{3+}. On the other hand, the average Sb–O bond lengths are nearly constant (∼2.00 Å). This value is equal to the bond length calculated from Shannon's ionic radii [36].

3.2. Paramagnetic behavior

Fig. 5 shows the temperature dependence of magnetic susceptibility of Pr_3SbO_7. Paramagnetic behavior was observed down to 1.8 K, i.e., no magnetic interaction was found in the experimental temperature range. In the inset, the reciprocal magnetic susceptibility was plotted against temperature. The susceptibility follows the Curie–Weiss law in the temperature range between 200 and 400 K. Magnetic susceptibility measurements for other Ln_3SbO_7 compounds also show that *Ln* = Sm, Eu, Er, Tm, and Yb compounds exhibit paramagnetic behavior down to 1.8 K. The effective magnetic moments (μ_{eff}) and Weiss constants (θ) are determined in the temperature range

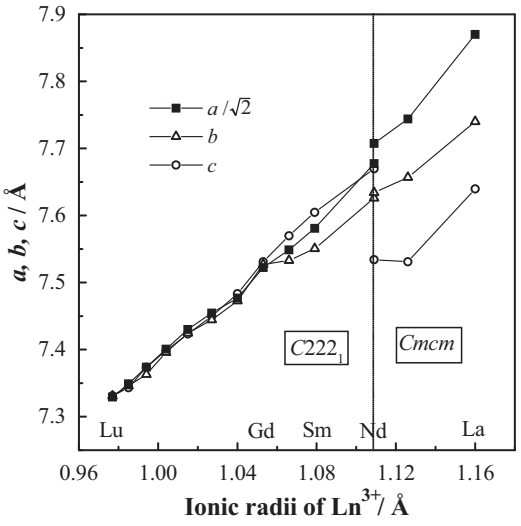

Fig. 3. Variation of lattice parameters for Ln_3SbO_7 with the ionic radius of Ln^{3+} in 8-coordination.

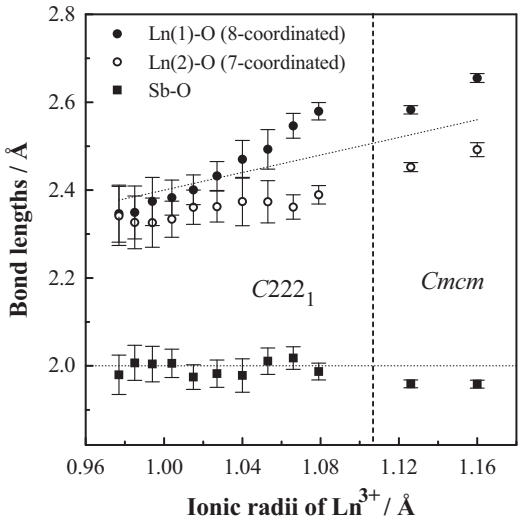

Fig. 4. Variation of *Ln*–O and Sb–O bond lengths with the ionic radius of Ln^{3+} in 8-coordination.

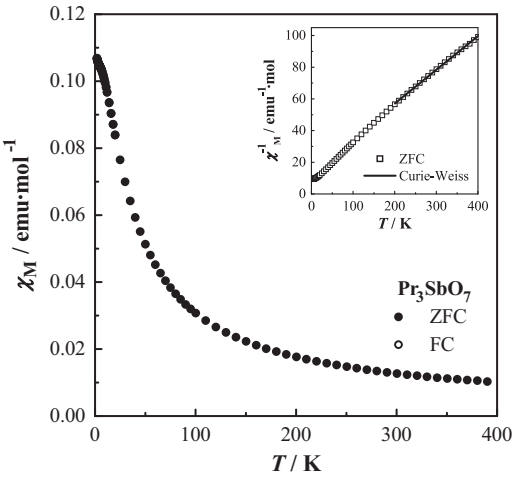

Fig. 5. Temperature dependence of the magnetic susceptibility for Pr_3SbO_7. The inset shows the reciprocal susceptibility vs. temperature curve. The solid line is the Curie–Weiss fitting.

between 200 and 400 K, and they are listed in Table 3. The effective magnetic moments are very close to the moments calculated for free Ln^{3+} ions. The negative Weiss constants indicate that the predominant magnetic interaction between Ln^{3+} ions is antiferromagnetic. If the magnetic susceptibility measurements were carried out furthermore below 1.8 K, these compounds should show an antiferromagnetic transition.

Fig. 6 depicts the temperature dependence of the magnetic susceptibility for Sm_3SbO_7 and Eu_3SbO_7. These compounds show the well-known van Vleck paramagnetism caused by the behavior of isolated Sm^{3+} and Eu^{3+} ions, respectively [37].

3.3. Magnetic ordering

Magnetic transitions have been observed for *Ln* = Nd, Gd–Ho compounds. Their transition temperatures are also listed in Table 3.

3.3.1. Gd_3SbO_7

Fig. 7 shows the temperature dependence of the magnetic susceptibility of Gd_3SbO_7. An antiferromagnetic transition has been observed at 2.6 K, and there is no divergence between the ZFC and FC susceptibilities below this temperature.

Table 3
Structure and magnetic properties of Ln_3SbO_7 (*Ln* = La–Lu).

Ln	Space group	Magnetic properties	μ_{eff}/μ_B	μ_{cal}/μ_B	θ(K)	T_N(K)
La	*Cmcm*	Diamagnetic	–	–	–	–
Pr	*Cmcm*	Paramagnetic	3.48	3.58	−60	–
Nd	$C222_1$	Antiferromagnetic	3.73	3.62	−7.8[c,a]	2.5,3.0
Sm	*Cmcm*, $C222_1$	van Vleck	1.58[a,b]	1.55[b,c]	–	–
Eu	$C222_1$	van Vleck	3.38[a,b]	3.40[b,c]	–	–
Gd	$C222_1$	Antiferromagnetic	7.96	7.94	−9.2	2.6
Tb	$C222_1$	Antiferromagnetic	9.53	9.72	−13.7	3.0
Dy	$C222_1$	Antiferromagnetic	10.4	10.63	−8.1	3.2
Ho	$C222_1$	Antiferromagnetic	10.6	10.58	−13.4	2.2
Er	$C222_1$	Paramagnetic	9.26	9.59	−9.7	–
Tm	$C222_1$	Paramagnetic	7.72	7.55	−4.6[c]	–
Yb	$C222_1$	Paramagnetic	4.72	4.54	−1.83[c]	–
Lu	$C222_1$	Diamagnetic	–	–	–	–

μ_{eff}: experimental values, μ_{cal}: calculated moments for Ln^{3+}.
[a] Observed values at room temperature.
[b] Calculated values by van Vleck [37].
[c] Values determined at low temperature regions.

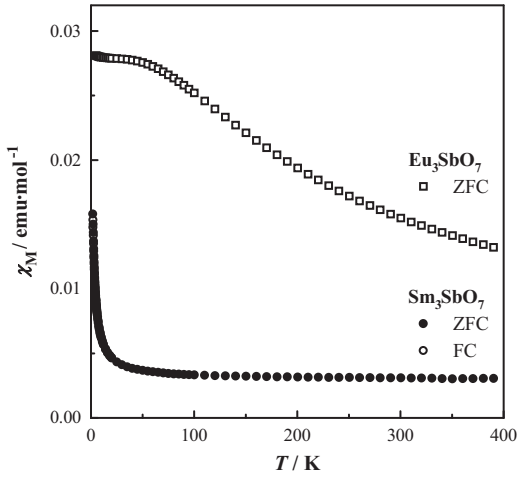

Fig. 6. Temperature dependences of the magnetic susceptibility for Sm_3SbO_7 and Eu_3SbO_7.

In order to obtain the information about the low-temperature magnetic behavior, specific heat measurements were performed down to 0.4 K. Fig. 8 shows the temperature dependence of the specific heat (C_p) divided by temperature (C_p/T) for Gd_3SbO_7. A specific heat anomaly has been observed at 2.6 K, which corresponds to the results by magnetic susceptibility measurements. Below this temperature, the specific heat increases with decreasing temperature, indicating the existence of another magnetic anomaly below 0.4 K. To evaluate the magnetic contribution to the specific heat (C_{mag}), we have to subtract the contribution of lattice specific heat (C_{lat}) from the total specific heat ($C_{mag} = C_p - C_{lat}$). The lattice specific heat was estimated by using the data for a diamagnetic compound La_3NbO_7 (the solid line of Fig. 8). The magnetic specific heat below 0.4 K was extrapolated by the relation $C_{mag} \propto T^3$ from the spin-wave model for the antiferromagnet [38] (the dotted line of Fig. 8). From the temperature dependence of the magnetic specific heat, the magnetic entropy change for Gd_3SbO_7 (S_{mag}) is calculated by the relation $S_{mag} = \int (C_{mag}/T)\,dT$. Its temperature dependence is also shown in Fig. 8. The total magnetic entropy change is ~50 J/mol K, and this value is close to $3R \ln 8 = 51.9$ J/mol K. The results indicate that all the Gd^{3+} ions contribute to the antiferromagnetic

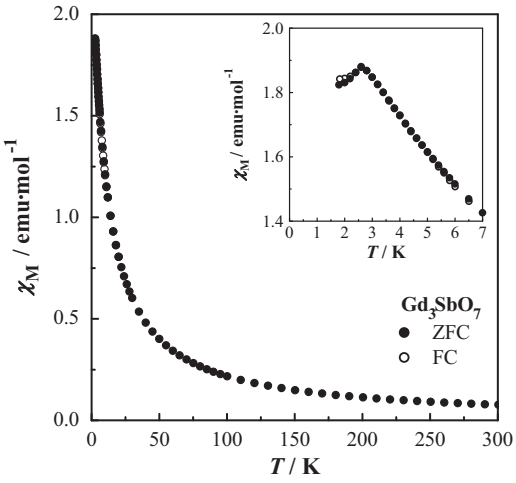

Fig. 7. Temperature dependence of the magnetic susceptibility for Gd_3SbO_7. The inset shows the detailed temperature dependence below 7 K.

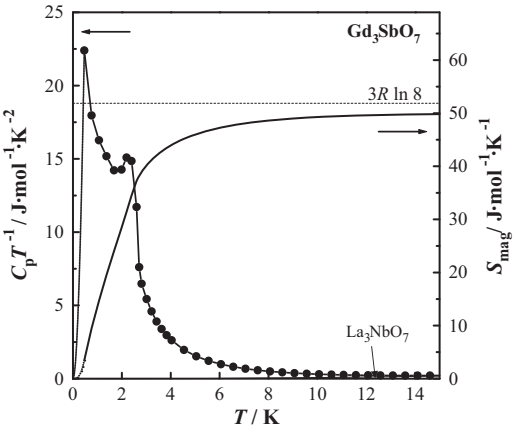

Fig. 8. Temperature dependence of C_p/T and S_{mag} for Gd_3SbO_7.

transition and that the ground state of the Gd^{3+} ions is still eight-degenerate ($^8S_{7/2}$) without crystal field splitting.

As shown in Fig. 8, it is difficult to divide the magnetic entropy data into two anomalies. However, it is clear that the magnetic entropy change due to the magnetic anomaly at a lower temperature is larger than that at a higher temperature (2.6 K). In the Gd_3SbO_7, the Gd^{3+} ions occupy two crystallographic sites, the 8-coordinated Gd(1) site (4*b*) and 7-coordinated Gd(2) site (8*c*), with the 1:2 ratio. Therefore, we believe that the magnetic transition at 2.6 K is due to the antiferromagnetic ordering of the 8-coordinated Gd(1) ions and that the magnetic anomaly at the lower temperature ($T<0.4$ K) is ascribable to the magnetic interactions of the 7-coordinated Gd(2) ions, i.e., Gd^{3+} ions occupying the 4*b* and 8*c* sites individually order in the Gd_3SbO_7 compound. Similar "two-step" magnetic transitions have been found for Ln_3TaO_7 (Ln = Nd, Tb) [24] and Ln_3NbO_7 (Ln = Nd, Tb) [39].

3.3.2. Dy_3SbO_7

The temperature dependence of the magnetic susceptibility of Dy_3SbO_7 is shown in Fig. 9. A clear antiferromagnetic transition has been observed at 3.2 K. The inset of Fig. 9 shows the reciprocal susceptibility versus temperature curve and the Curie–Weiss fitting. For this compound, specific heat measurements were also performed down to 0.4 K. The specific heat divided by temperature (C_p/T) is shown in Fig. 10. A clear λ-type specific heat anomaly has been observed at 3.2 K, at which the magnetic susceptibility shows antiferromagnetic behavior. The magnetic specific heat was estimated by subtracting the contribution of the lattice specific heat from the total specific heat in the same way as is the case for Gd_3SbO_7. The magnetic entropy change is calculated from the specific heat data by using the equation $S_{mag} = \int(C_{mag}/T)\,dT$, and it is obtained to be 17.1 J/mol K. This value is quite near to $3R \ln 2 = 17.3$ J/mol K. The ground multiplet of Dy^{3+} ion, $^6H_{15/2}$ splits into eight Kramers'doublets due to the effect of the crystal field with low symmetry. The experimental results indicate that the ground Kramers' doublets for three Dy^{3+} ions cause the antiferromagnetic ordering.

3.3.3. Nd_3SbO_7, Tb_3SbO_7, Ho_3SbO_7

For Tb_3SbO_7 and Ho_3SbO_7, a clear antiferromagnetic transition has been observed at 3.0 and 2.2 K, respectively. There is no divergence between ZFC and FC susceptibilities. Although Funnell et al. reported a possibility of magnetically frustrated system for Ho_3SbO_7 and Dy_3SbO_7 [34], there is no appearance of magnetic frustration. Fig. 11 shows the temperature dependence of magnetic susceptibility of Nd_3SbO_7, indicating the antiferromagnetic transition at 3.0 K. In addition, another magnetic anomaly was observed at 2.5 K. No divergence between ZFC and

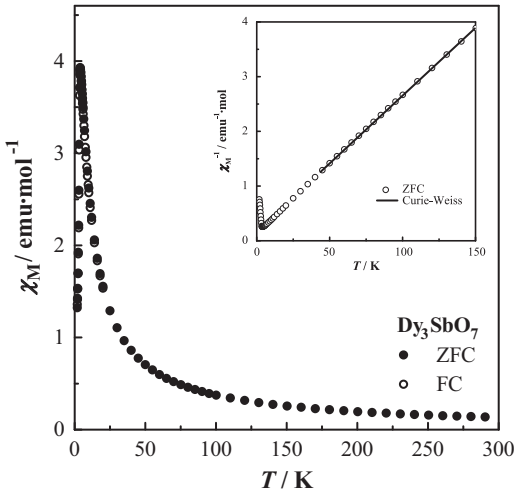

Fig. 9. Temperature dependence of the magnetic susceptibility for Dy_3SbO_7. The inset shows the reciprocal susceptibility vs. temperature curve. The solid line is the Curie–Weiss fitting.

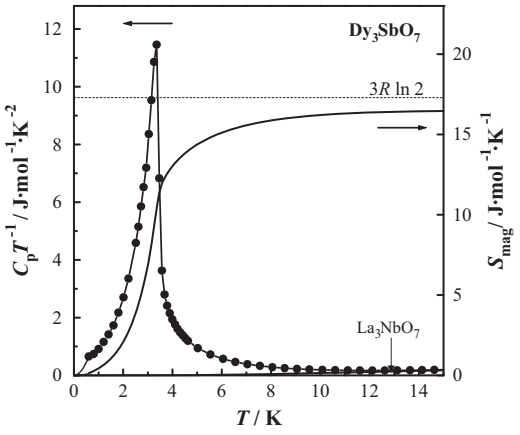

Fig. 10. Temperature dependence of C_p/T and S_{mag} for Dy_3SbO_7.

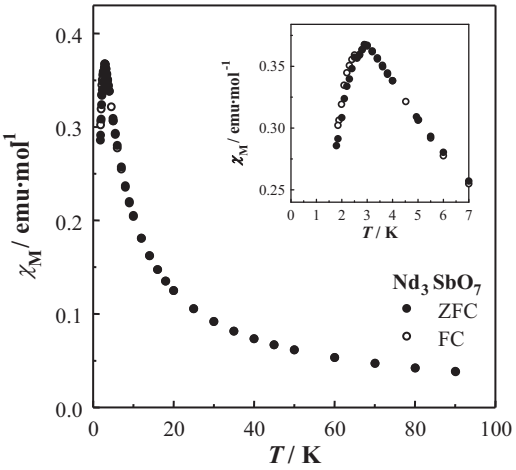

Fig. 11. Temperature dependence of the magnetic susceptibility for Nd_3SbO_7. The inset shows its detailed temperature dependence below 7 K.

FC susceptibilities was found below these transition temperatures. This is due to the fact that two phases of Nd_3SbO_7 possibly have different Neel temperatures.

4. Summary

Rare earth antimonates Ln_3SbO_7 (Ln = Nd, Gd–Ho) show an antiferromagnetic transition at 2.2–3.2 K. Measurements of the specific heat down to 0.4 K for Gd_3SbO_7 indicate that the 8-coordinated Gd ions antiferromagnetically order at 2.6 K and with furthermore decreasing temperature, the 7-coordinated Gd ions show a magnetic anomaly, i.e., the magnetic moments at the two crystallographic sites order individually.

Acknowledgments

This work was supported by Grant-in-aid for Scientific Research, no. 20550052, from the Ministry of Education, Science, Sports, and Culture of Japan.

References

[1] H.J. Rossell, J. Solid State Chem. 27 (1979) 115–122.
[2] A. Kahn-Harari, L. Mazerrolles, D. Michel, F. Robert, J. Solid State Chem. 116 (1995) 103–106.
[3] F.P.F. Van Berkel, D.J.W. IJdo, Mater. Res. Bull. 21 (1986) 1103–1106.
[4] W.A. Groen, F.P.F. Van Berkel, D.J.W. IJdo, Acta Crystallogr. Sect. C 43 (1986) 2262–2264.
[5] P. Khalifah, R.W. Erwin, J.W. Lynn, Q. Huang, B. Batlogg, R.J. Cava, Phys. Rev. B 60 (1999) 9573–9578.
[6] P. Khalifah, Q. Huang, J.W. Lynn, R.W. Erwin, R.J. Cava, Mater. Res. Bull. 35 (2000) 1–7.
[7] F. Wiss, N.P. Raju, A.S. Wills, J.E. Greedan, Int. J. Inorg. Mater. 2 (2000) 53–59.
[8] B.P. Bontchev, A.J. Jacobson, M.M. Gospodinov, V. Skumryev, V.N. Popov, B. Lorenz, R.L. Meng, A.P. Litvinchuk, M.N. Iliev, Phys. Rev. B 62 (2000) 12235–12240.
[9] D. Harada, Y. Hinatsu, J. Solid State Chem. 158 (2001) 245–253.
[10] D. Harada, Y. Hinatsu, Y. Ishii, J. Phys. Condens. Matter 13 (2001) 10825–10836.
[11] D. Harada, Y. Hinatsu, J. Solid State Chem. 164 (2002) 163–168.
[12] R. Lam, F. Wiss, J.E. Greedan, J. Solid State Chem. 167 (2002) 182–187.
[13] W.R. Gemmill, M.D. Smith, H.-C. zur Loye, Inorg. Chem. 43 (2004) 4254–4261.
[14] N. Ishizawa, K. Hiraga, D. du Boulay, H. Hibino, T. Ida, S. Oishi, Acta Crystallogr. E 62 (2006) i13–i16.
[15] G. Wltschek, H. Paulus, I. Svoboda, H. Ehrenberg, H. Fuess, J. Solid State Chem. 125 (1996) 1–4.
[16] R. Lam, T. Langet, J.E. Greedan, J. Solid State Chem. 171 (2002) 317–323.
[17] Y. Hinatsu, M. Wakeshima, N. Kawabuchi, N. Taira, J. Alloys Compd. 374 (2004) 79–83.
[18] J.R. Plaisier, R.J. Drost, D.J.W. IJdo, J. Solid State Chem. 169 (2002) 189–198.
[19] W.R. Gemmill, M.D. Smith, Y.A. Mozharivsky, G.J. Miller, H.-C. zur Loye, Inorg. Chem. 44 (2005) 7047–7055.
[20] J.G. Allpress, H.J. Rossell, J. Solid State Chem. 27 (1979) 105–114.
[21] Y. Yokogawa, M. Yoshimura, S. Somiya, Mater. Res. Bull. 22 (1987) 1449–1456.
[22] Y. Yokogawa, M. Yoshimura, S. Somiya, Solid State Ionics 28 (1988) 1250–1253.
[23] J.F. Vente, R.B. Helmholdt, D.J.W. IJdo, J. Solid State Chem. 108 (1994) 18–23.
[24] M. Wakeshima, Y. Hinatsu, J. Phys. Condens. Matter 16 (2004) 4103–4120.
[25] J.F. Vente, D.J.W. IJdo, Mater. Res. Bull. 26 (1991) 1255–1262.
[26] H. Nishimine, M. Wakeshima, Y. Hinatsu, J. Solid State Chem. 177 (2004) 739–744.
[27] J.E. Greedan, N.P. Raju, A. Wegner, P. Gougeon, J. Padiou, J. Solid State Chem. 129 (1997) 320–327.
[28] N. Barrier, P. Gougen, Acta Crystallogr. E 59 (2003) i22–i24.
[29] H. Nishimine, M. Wakeshima, Y. Hinatsu, J. Solid State Chem. 178 (2005) 1221–1229.
[30] N. Barrier, P. Gougen, Acta Crystallogr. C 63 (2003) i102–i104.
[31] N. Ishizawa, K. Tateishi, S. Kondo, T. Suwa, Acta Crystallogr. 47 (2006) 558–566.
[32] D.K. Nath, Inorg. Chem. 9 (1970) 2714–2718.
[33] J.P. Faurie, G. Boulon, C. Delaigue, J. Solid State Chem. 17 (1976) 7–14.
[34] T. Fennell, S.T. Bramwell, M.A. Green, Can. J. Phys. 79 (2001) 1415–1419.
[35] F. Izumi, T. Ikeda, Mater. Sci. Forum 198 (2000) 321–324.
[36] R.D. Shannon, Acta Crystallogr. Sect. A 32 (1976) 751–767.
[37] J.H. Van Vleck, Theory of Electric and Magnetic Susceptibilities, Oxford, Clarendon, 1932.
[38] S.J. Joshua, A.P. Cracknell, Phys. Lett. A 28 (1969) 562–563.
[39] Y. Doi, Y. Harada, Y. Hinatsu, J. Solid State Chem. 182 (2009) 709–715.